Chemical routes to materials

Hydrogen peroxide LSPR sensing with unoxidised CuNPs-Tween® 60

Giorgio Giuseppe Carbone[1,*] , Daniela Manno[2], Antonio Serra[2], and Alessandro Buccolieri[2]

[1] Department of Biological and Environmental Sciences and Technologies (DiSTeBA), University of Salento, 73100 Lecce, Italy
[2] Department of Mathematics and Physics "E. De Giorgi", University of Salento, 73100 Lecce, Italy
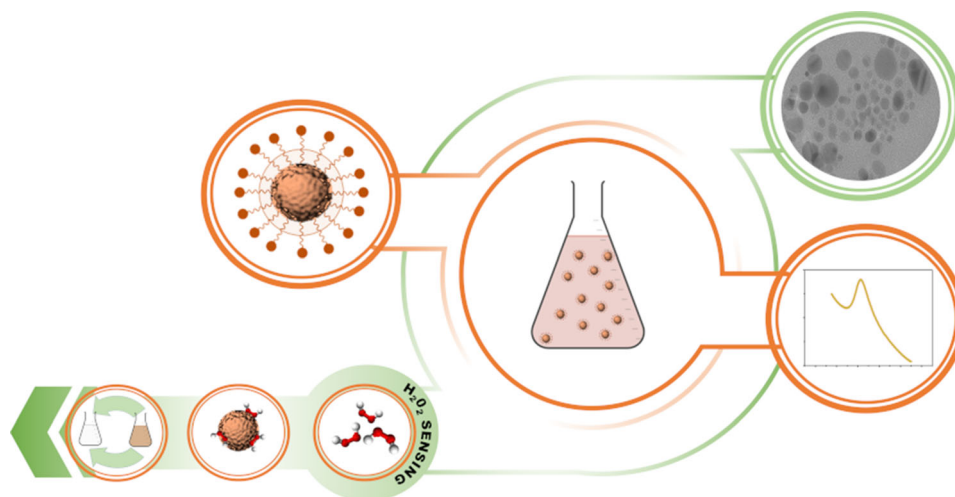
ABSTRACT

Copper nanoparticles (CuNPs) as well as those of other noble metals show unique features that are not observed in bulk copper. Despite the enormous potential of CuNPs, their use is limited by their susceptibility to oxidation during and after synthesis. Here, an innovative method based on wet synthesis protocol was developed to produce an aqueous colloidal solution of CuNPs capped with Tween® 60 (Polyoxyethylene sorbitan monostearate) capable of being stable and non-oxidised for several months. The CuNPs colloidal solution was tested for the detection of hydrogen peroxide (H_2O_2) showing a detection limit of 10^{-11} M. This result may provide the basis for the design of a rapid, practical, and easy-to-use colorimetric sensor to detect H_2O_2 in the future.

GRAPHICAL ABSTRACT

Introduction

H_2O_2 is a molecule that belongs to a class of compounds known as reactive oxygen species (ROS) [1]. Most of the ROS in human body are produced by mitochondria and eliminated through a process known as ROS homeostasis [2]. Hydrogen peroxide is used in many fields such as food processing [3], pharmaceuticals [4], clinical and environmental [5]. If an excess of H_2O_2 is introduced in human body, it could not be properly metabolized, leading to a pathological condition known as oxidative stress [6].

For these reasons, there is the need of rapid and efficient hydrogen peroxide detection systems. Many analytical methods for H_2O_2 determination have been reported in the scientific literature, but most of them are based on the immobilization of a protein, such as *horseradish peroxidase* (HRP) [7–11]. The main disadvantage of these methods is the protein degradation, which in the long term makes biosensor detection inaccurate [12]. For this reason, there has been strong interest in non-enzymatic H_2O_2 sensors in recent years, particularly those based on metal nanoparticles [13]. At the nanoscale, when a metal nanoparticle is irradiated by appropriate UV–Vis radiation its surface electrons oscillate collectively. This phenomenon is known as localized surface plasmonic resonance (LSPR). Experimentally, LSPR is observed with the formation of a characteristic peak in the light absorption spectrum. The peak position is affected by morphological, structural and chemical characteristics of metal nanoparticles [14]. Furthermore, the LSPR phenomenon strongly depends on the distance between metal nanoparticles. Such distance is influenced by the interaction between analytes and metal nanoparticles modifies, thus allowing the use of LSPR absorption as an analytical property for the optical and colorimetric detection of various chemical species [15]. Currently, most of the plasmonic nanoparticle synthesis methods focus on precious metals such as Au [16] and Ag [17]. However, the high cost of these metals limits the development of economic sensors and their use in large-scale production.

In this context, copper has attracted wide interest in the field of LSPR-based devices research due to its significantly lower cost compared to other noble metals.

There are several methods of copper nanoparticles (CuNPs) synthesis, including thermal reduction [18], vapour deposition [19], radiation methods [20], microemulsion [21] and laser ablation [22].

Among these methods, the wet synthesis method is found to be simple and most versatile for metal nanoparticles including copper once [23].

In the present work, a low-cost wet synthesis method was developed to produce a metallic CuNPs colloidal solution capable of detecting small H_2O_2 concentrations.

A limitation in the synthesis of metallic CuNPs colloidal solutions and in general in the synthesis of metallic nanoparticles colloidal solutions regards their aggregation after preparation.

One of the most widely used strategies to minimise the aggregation of nanoparticles in solution is to coat their surface with a "physical barrier" (steric stabilisation) [24]. In this regard, polymers [25], including Tween® 60 used in the present work, have proved to be effective coating materials for increasing the stability of nanoparticles in colloidal solutions.

Tween® 60 belongs to the category of polysorbates, which are an important type of non-ionic surfactants widely used in the pharmaceutical industry due to their high biocompatibility [26]. This surfactant is a copolymer obtained by combining sorbitol with ethylene oxide esterified with fatty acids. The ability of Tween® 60 to reduce the aggregation of the nanoparticles is due to its oligo (ethylene glycol) moieties, which increase the steric stabilisation of the colloidal solution [27].

Another limitation in the synthesis of CuNPs regards their oxidation susceptibility during and after preparation [28]. This makes the synthesis of metallic CuNPs difficult without providing an inert environment of Ar or N_2.

The oxidation problems of CuNPs can be avoided by using different protective agents such as polymers [29]. In our case, Tween® 60 alone proved to be not sufficient in protecting CuNPs from oxidation. For this reason, we used a natural antioxidant, ascorbic acid, during the synthesis of our CuNPs. The antioxidant properties of ascorbic acid are well known and derive from its ability to limit the action of free radicals and reactive oxygen molecules, which are often present in the reaction environment [30].

Overall, the combined action of Tween® 60 and ascorbic acid enabled us to synthesise a stable metallic CuNPs colloidal solution through chemical reduction in an aqueous environment without employing an inert atmosphere.

Experimental

Materials

Copper (II) chloride dihydrate ($CuCl_2 \cdot 2H_2O$, 99%), sodium borohydride ($NaBH_4$, 99%), Tween® 60 (Polyoxyethylene sorbitan monostearate, estimated molar weight 1309 g mol^{-1}) and L-ascorbic acid ($C_6H_8O_6$, 99%) were purchased from Sigma-Aldrich®. Hydrogen peroxide 30% (v v^{-1}) as analyte was purchased from Chembid®. Deionized water was obtained by a Zener Up 900 (Human Corporation) water purification system and used throughout the experiments.

Instruments

Ultraviolet–visible spectroscopy

UV–Vis spectrophotometer model T80 (Pg Instruments Ltd) was employed to study: (a) the optical characteristics of the CuNPs colloidal solution by recording its absorbance in the range between 400 and 800 nm; (b) the CuNPs response to different H_2O_2 concentrations by acquiring the absorption spectrum of the solution every 5, 10 and 15 min after the analyte addition.

Transmission electron microscopy (TEM)

TEM images and electron diffraction patterns were recorded using Hitachi 7700 transmission electron microscope operated at 100 kV. This acceleration voltage was settled to obtain a sufficient resolution and minimal radiation damage of the material. Specimens for TEM observations were prepared by drop-casting the freshly CuNPs solutions onto standard carbon-supported 600-mesh copper grid previously coated with amorphous carbon. The nanoparticles were fixed to the grid by allowing the solvent to evaporate at room temperature for 24 h.

TEM was also used to obtain selected area electron diffraction (SAED) images from chosen areas of approximately 10^3 nm in diameter. The diffraction images were processed using the PASAD plug-in integrated in the Gatan Microscopy Suite® software.

Scheme 1 Illustration of the copper nanoparticles synthesis process steps and of the observed solution colour changes.
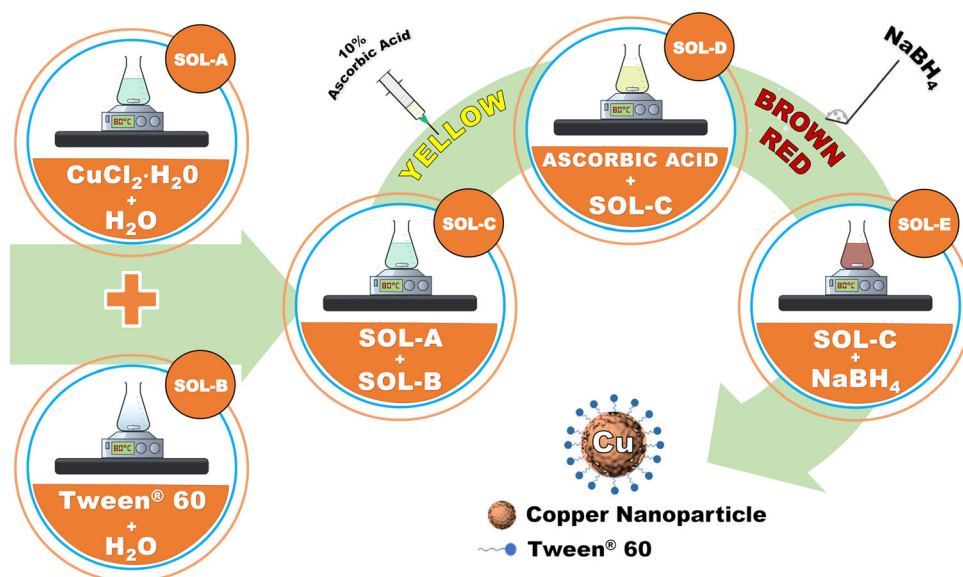
## Synthesis of copper nanoparticles coated with Tween® 60

The synthesis steps of copper nanoparticles are shown in Scheme 1. In a typical synthesis, 0.05 g of $CuCl_2 \cdot 2H_2O$ was dissolved into 40 mL of deionized water to obtain a light green solution. This solution was heated to 80 °C (SOL-A) under magnetic stirring. Meanwhile, 0.8 g of Tween® 60 was dissolved in 40 mL of water and heated to 80 °C (SOL-B) under magnetic stirring. The amount of Tween® 60 was optimized to maximize the number of CuNPs in suspension and to improve the stability of the solution over time. SOL-A and SOL-B solutions were mixed to obtain a new solution (SOL-C) that was kept at 80 °C under magnetic stirring. The colour of this solution was like that of SOL-A. Finally, 4 mL of 10% aqueous solution of ascorbic acid was added to SOL-C. This new solution (SOL-D) was kept at 80 °C under magnetic stirring. After a few minutes, the solution changes its colour from light green to transparent. One hour later there was a new change of colour of the solution, from transparent to straw yellow. At this point, 0.15 g of $NaBH_4$ was added to SOL-D, which instantly changed colour from straw yellow to reddish brown. This colour is typical of colloidal solutions of copper nanoparticles. The yield of the CuNPs synthesis reaction was calculated gravimetrically and ranged from 60 to 66%.

Results and discussion

Formation of copper nanoparticles

The CuNPs formation mechanism of copper nanoparticles using Tween® 60 as a stabilizing agent in aqueous solution is proposed in Scheme 2. The first step of this process is the formation of Tween® 60 micelles capable of incorporating copper ions.

Since copper ions were present in our solution, it was reasonable to assume that they were incorporated into the micelles. Subsequently, the addition of $NaBH_4$ as a reducing agent instantaneously triggered the reduction process of the copper ions, according to the reaction:

$$Cu^{2+} + 2BH_4^- \rightarrow Cu + H_2 + B_2H_6$$
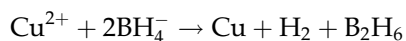
The electron transfer from borohydride anions to copper ions led to the nucleation of copper atoms within the Tween® 60 micelles. Copper nuclei tended to coalesce inside the micelles led to the formation of spherical copper nanoparticles. The strong micellar effect suppressed the directional growth of CuNPs, preventing the formation of any other type of morphology.

Working in air, to avoid formation of copper oxide nanoparticles, ascorbic acid was added before the reducing agent. The antioxidant properties of ascorbic acid are well known. For example, Liu et al. have shown that ascorbic acid prevents the formation of copper oxide by decreasing the pH of the solution in which it is dissolved [31]. Ascorbic acid can reduce

Scheme 2 Proposed CuNPs formation process inside the Tween® 60 micelles.
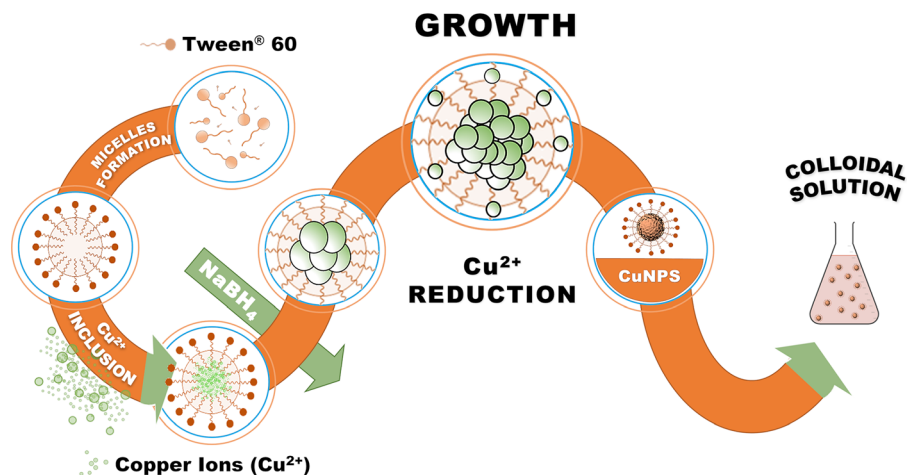
the oxidation state of metal ions by oxidising itself according to the reaction:

Ascorbic acid ⇌ Dehydroascorbic acid + $2e^- + 2H^+$
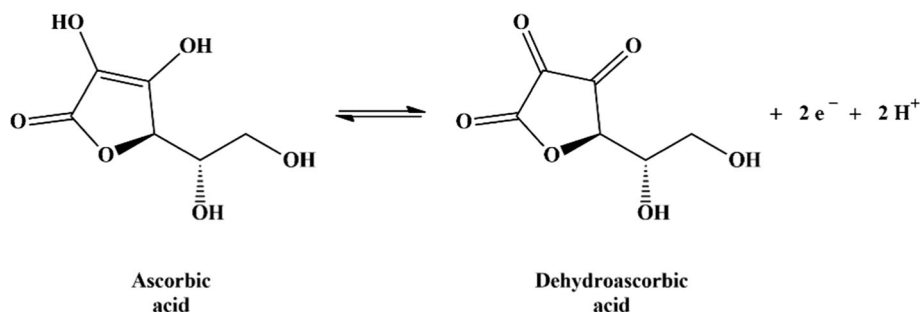
Another challenge encountered in the development of this synthesis protocol concerned the aggregation of micelles. This phenomenon was predominant when the synthesis was carried out at room temperature. At this temperature, the micelles tended to interact with each other, increasing their size and consequently leading to the formation of larger nanoparticles. To limit the aggregation of the micelles, the solution was kept at a temperature of 80 °C throughout the synthesis.

The influence of temperature on the thermodynamic parameters describing the molecular order of non-ionic surfactants such as Tween® 60 was the object of numerous studies. For example, Szymczyk et al. 2018 observed that as the temperature increased, the intermolecular cohesive forces between the micelles decreased [32]. Consequently, as the temperature increases, the melting of the micelles is limited. The properties of the synthesized CuNPs colloidal solution were analyzed using UV–Vis spectrophotometry and TEM.

Optical and structural characterization of CuNPs-Tween® 60 solution

UV–Vis spectrophotometry was used to study the optical characteristics of the CuNPs solution since noble metal nanostructures like copper once exhibited localized surface plasmon resonance (LSPR) bands at different frequencies. As shown in Fig. 1 (orange curve), the colloidal solution of CuNPs had a broad LSPR peak in the spectral range between 500 and 650 nm, with an absorption maximum located at 590 nm. The position of this peak indicates the formation of a colloidal solution with nanometer-sized copper nanoparticles.

We measured the absorption spectrum of the CuNPs solution after one month, to test its stability. The spectrum remained unchanged as shown in Fig. 1 (green curve), proving that Tween® 60 prevented precipitation, further aggregation and together with ascorbic acid oxidation of copper nanoparticles.
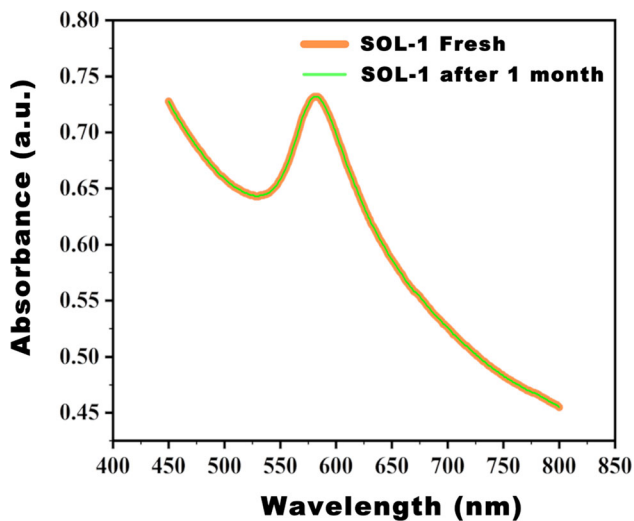
Figure 1 UV–visible absorption spectra of CuNPs solution fresh and one month after preparation. The LSPR peak is located at 590 nm.

The CuNPs morphology was studied by TEM. Figure 2a shows a typical bright-field image of the CuNPs colloidal solution. By analysing the image, it can be deduced that all the nanoparticles are approximately spherical in shape. To obtain the average size of the nanoparticles in solution and their size distribution, 20 TEM images were acquired from casual sample regions and processed with the Digital Micrograph® tool of the Gatan Microscopy Suite® software, obtaining the histogram shown in Fig. 2b. The largest part of CuNPs has an average diameter of 8 ± 1 nm. There was also a second pool of CuNPs with an average diameter of 25 ± 2 nm.

TEM was also used to highlight the crystalline nature of CuNPs using the SAED technique. In order to obtain statistically significant results, ten SAED images were analysed for each sample and processed using the PASAD plug-in integrated in the Gatan Microscopy Suite® software.

An electron diffraction image acquired over the sample area observed in Fig. 2a is shown in Fig. 3.

The SAED pattern is characterised by four well-defined diffraction rings, which correspond to the lattice planes (1 1 1), (2 0 0), (2 2 0) and (3 1 1) of a copper metal crystal with an FCC (Face-Centred Cubic) structure, respectively [RRUFF™ Project, RRUFF ID: R061078]. These results allow us to state that the nanoparticles were exclusively composed by metallic copper with no trace of oxides.

TEM and SAED analyses were unable to provide information on the capping of Tween® 60, probably because to its reduced thickness.

However, if the surface of the nanoparticles is coated with Tween® 60, this interaction can be detected by a shift towards longer wavelengths of the absorption spectrum of an uncapped CuNPs colloidal solution. In our case, since we were unable to synthesize an aqueous colloidal solution of metallic CuNPs without capping, the spectrum of this solution was obtained through a simulation.

In order to derive the size-dependent dielectric function to be used in the simulation, the characteristic LSPR absorption peak of our CuNPs solution was analysed according to both the light scattering theory proposed by Mie [33] and the free electron theory of Drude [34].

As evidenced by TEM analysis, our CuNPs are dual-dispersed; then, according to Mie formalism, the absorption coefficient α_j due to particles of diameter d_j, dispersed in water having permittivity $\varepsilon_m = 1.3$ at 300 K [35], is (Eq. 1):

Figure 2 **a** TEM image of the CuNPs solution. **b** Size distribution of the copper nanoparticles.
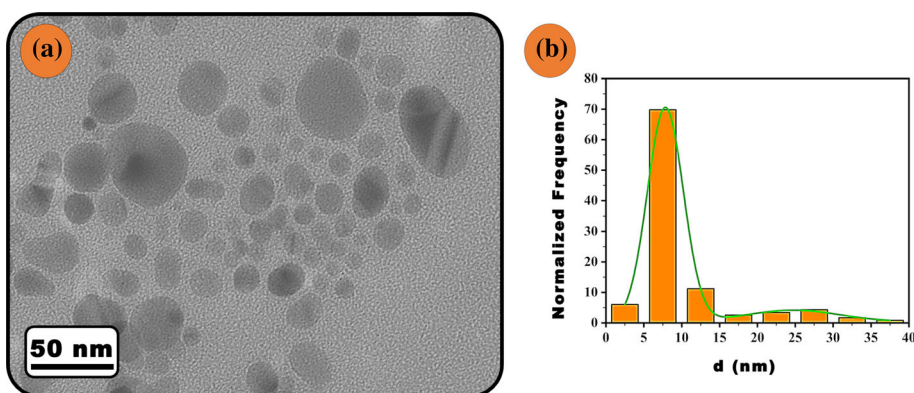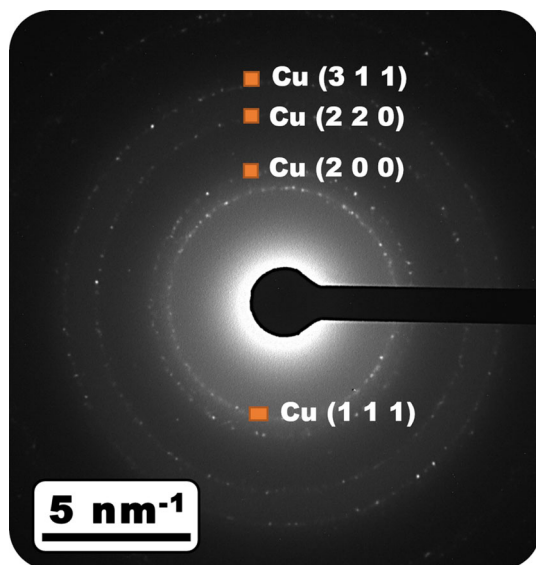
Figure 3 SAED pattern of the CuNPs solution. The orange squares represent the reflections originated by the CuNPs.

$$\alpha_j = \frac{18\pi f_j \varepsilon_m^{\frac{3}{2}} \varepsilon_{2j}}{\lambda (\varepsilon_{1j} + 2\varepsilon_m)^2 + \varepsilon_{2j}^2} \tag{1}$$

where f_j is the volume fraction of the metal particles with diameter d_j, λ is the photon wavelength, and $\varepsilon_j = \varepsilon_{1j} + i\varepsilon_{2j}$ is the dielectric function of the copper nanoparticles. To consider that there was a finite distribution of particle size, we may write the total absorption coefficient (α) as (Eq. 2):

$$\alpha = \sum_j \alpha_j \tag{2}$$

The volume fraction of the silver nanoparticles is given by (Eq. 3):

$$fw_j = f_j \tag{3}$$

where w_j is the weight factor for particles with diameter d_j and is given by (Eq. 4):

$$w_j = \frac{d_j^3 n_j}{\sum_j d_j^3 n_j} \tag{4}$$

where d_j is the diameter of the CuNPs, and n_j is the number of CuNPs of diameter d_j. Hence, it is possible to express the size-dependent dielectric function ε_j according to the relation (Eq. 5):

$$\varepsilon_j(\omega) = \varepsilon_{\text{bulk}}(\omega) - \frac{\left(\frac{\omega_P}{\omega}\right)^2}{1 + \left(\frac{2v_F}{\omega d_j}\right)^2} + i\frac{2v_F \omega_P^2}{\omega^3 d_j} \tag{5}$$

where ω is the photon frequency, v_f is the Fermi velocity, and $\varepsilon_{\text{bulk}}$ is the electrical permittivity corresponding to the inter-band transitions, which is equal to (Eq. 6):

$$\varepsilon_{\text{bulk}} = 1 - \frac{\omega_P^2}{(\omega^2 + i\omega\gamma_{\text{free}})} \tag{6}$$

With the damping constant of the electron oscillatory movement $\gamma_{\text{free}} = 3 \cdot 10^{13}$ s^{-1}.

We simulated the experimental absorption data using Eq. 5 and considering a CuNPs solution consisting of 95% CuNPs having mean size of (8 ± 2) nm and 5% CuNPs having mean size of (25 ± 5) nm, a plasma frequency $\omega_{P0} = 3.7 \cdot 10^{15}$ rads^{-1} and a Fermi velocity $v_F = 1.38 \cdot 10^8$ cms^{-1}.

The simulated spectrum and that of our solution are reported in Fig. 4. The simulated spectrum shows an absorption peak at 585 while that of our solution is shifted towards the red by 5 nm. This shift indicates the formation of adsorbed layers of Tween® 60 around CuNPs [36].

The importance of the combined action of Tween® 60 and ascorbic acid

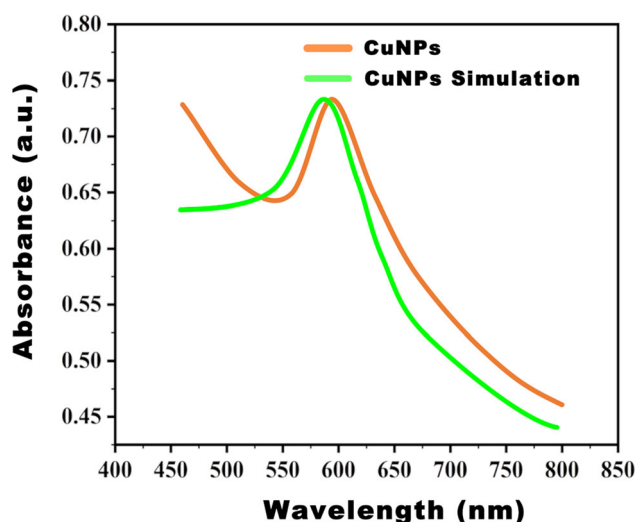In this study, to synthesise a colloidal solution of CuNPs that resists oxidation and aggregation over

Figure 4 Real UV–Vis absorption spectra of CuNPs-Tween® 60 (orange line) and simulated UV–Vis absorption spectra of CuNPs (green line).

time, the combined use of Tween® 60 and ascorbic acid was assumed to be essential. In order to evaluate this aspect, a new synthesised CuNPs solution with Tween® 60 and ascorbic acid (SOL-1) was compared with two solutions synthesised excluding in one the addition of ascorbic acid (SOL-2) and in the other the addition of Tween® 60 (SOL-3).

The three solutions were photographed immediately after synthesis (Fig. 5a) and after 24 h (Fig. 5b). In addition, to highlight the possible presence of CuNPs, UV–Vis spectra were acquired for each solution immediately after synthesis and after 24 h (Fig. 5c).

From the visual comparison of the newly synthesized solutions (Fig. 5a), only SOL-1 appears reddish brown, which is the typical colour of a colloidal solution of metallic CuNPs. The presence in SOL-1 of unoxidized CuNPs was also evidenced by a plasmonic peak at 590 nm in the UV–Vis spectrum shown in Fig. 5c. The UV–Vis spectrum remained unchanged even 24 h after synthesis (Fig. 5c). This agrees with what has already been described in the previous paragraph regarding the stability of the solution under study.

On the other hand, the colour of the remaining two solutions was markedly different from that of SOL-1. SOL-2 appeared blackish in colour (Fig. 5a), and this was assumed to be due to the oxidation of part of the metallic CuNPs in the newly synthesised solution. This hypothesis was confirmed by acquiring the UV–Vis spectrum of SOL-2 after synthesis (Fig. 5c).

In addition to the CuNPs plasmonic at 590 nm, there is a second peak around 300 nm attributable to the oxidised CuNPs [37]. 24 h after the synthesis of SOL-2, due to the oxidation of most of the metallic CuNPs, the intensity of the peak at around 300 nm increased while that at 590 nm decreased.

This increase in oxidised CuNPs can also be evidenced by the change in colour from blackish to viscous green of SOL-2 (Fig. 5b), which is the typical colour of an oxidised CuNPs solution [38]. To further confirm the presence of oxidised CuNPs in SOL-2, its SAED pattern was acquired 24 h after synthesis (Fig. 6a) and compared with that of SOL-1 also obtained 24 h after synthesis (Fig. 6b).

In order to obtain statistically significant results, ten SAED images were analysed for each sample and

Figure 5 **a** Pictures of the fresh SOL-1, SOL-2 and SOL-3 solutions. **b** Pictures of the SOL-1, SOL-2 and SOL-3 solutions after 24 h. **c** UV–Vis spectra of the three fresh/after 24 h solutions.
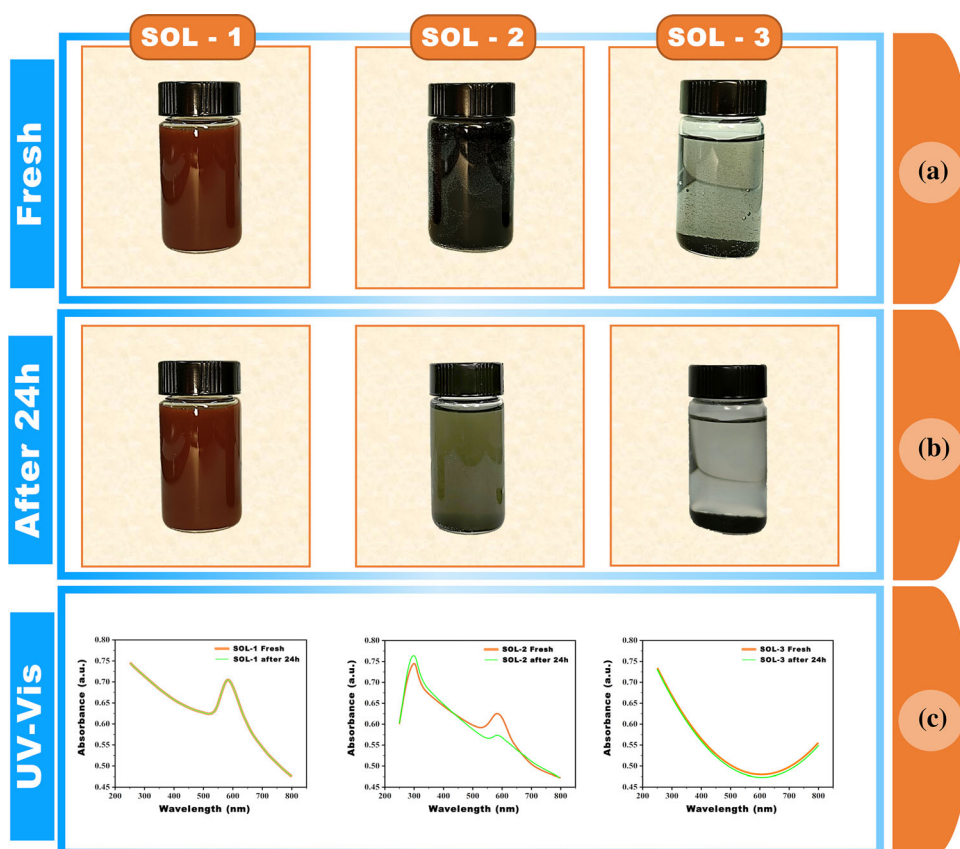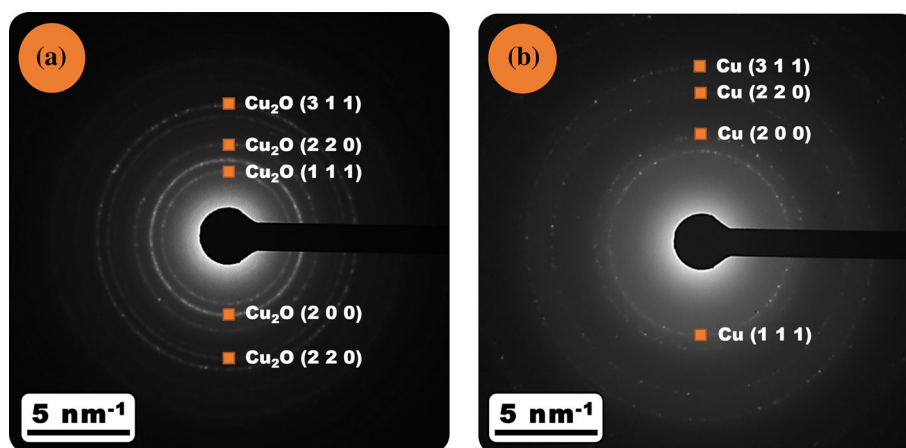
Figure 6 a SAED pattern of SOL-2. **b** SAED pattern of SOL-1. The orange squares represent the reflections originated in **a** by the oxidised CuNPs and in **b** by the CuNPs.

processed using the PASAD plug-in integrated in the Gatan Microscopy Suite® software.

While the SAED pattern of SOL-1 is characterised by four well-defined diffraction rings, which correspond to the lattice planes (1 1 1), (2 0 0), (2 2 0) and (3 1 1) of a copper metal crystal with an FCC (Face-Centred Cubic) that of SOL-2 is characterized by five diffraction rings with lattice indexes (1 1 1), (2 0 0), (2 2 0), (2 2 0) and (3 1 1) which is characteristic of oxidised CuNPs. These observations clearly show that CuNPs oxidise very quickly in the absence of ascorbic acid.

In the case of SOL-3, both suspended particles and a deposit at the bottom of the solution were already visible in the newly synthesised solution (Fig. 5a). 24 h after synthesis, the suspended particles also settled to the bottom, making the solution completely clear (Fig. 5b).

It is reasonable to assume that the formation of this sediment is due to CuNPs aggregation phenomena caused by the absence of the stabilising action of Tween® 60. The absence of CuNPs in solution was confirmed by acquiring the UV–Vis spectra of SOL-3 shown in Fig. 5c where no characteristic peak of CuNPs is evident.

All results prove that the combined action of Tween® 60 and ascorbic acid is crucial for our synthesis in order to obtain an aqueous solution of metallic CuNPs without employing an inert atmosphere that is stable over time and resistant to oxidation.

Evaluation of CuNPs solution as hydrogen peroxide sensor

1 mL of the CuNPs solution was placed in different cuvettes, and a different concentration of H_2O_2 from 10^{-11} to 1 M was added to each cuvette. The response of the CuNPs solution to each concentration was estimated by recording the UV–Vis spectrum of the solution every 5 min for 15 min at a fixed wavelength of 590 nm. This wavelength was used for each measurement as it corresponded to the absorption peak of the CuNPs solution.

Each acquisition cycle was repeated ten times using a new aliquot of the CuNPs stock solution. Therefore, the absorbance values (Abs_t) reported for each H_2O_2 concentration tested as a function of time are the average of ten different measurements. The estimated maximum error was 5%.

The recorded absorbance values (Abs_t) were normalised by dividing them by the absorbance value obtained before adding the analyte to each cuvette (Abs_0). Abs_t/Abs_0 as a function of time for each H_2O_2 concentration tested is shown in Fig. 7a.

As shown in Fig. 7a, the absorbance is time and concentration dependent. For each H_2O_2 concentration tested, the absorbance decreases with time and with a greater intensity as the H_2O_2 concentration increases. To the naked eye, the decrease in the absorption intensity after the addition of H_2O_2 is observed by the gradual decolourisation of the CuNPs solution. The greater the concentration of H_2O_2 used, the greater the intensity of discolouration.

As a result, 15 min after the addition of H_2O_2 at higher concentrations (e.g. 1 M or 0.1 M), the CuNPs solution became completely transparent. On the other

Figure 7 a Time-dependent change in normalised absorbance of CuNPs solution for each H_2O_2 concentration tested; **b** performance of the CuNPs solution expressed in terms of change in absorbance as a function of H_2O_2 concentration tested.
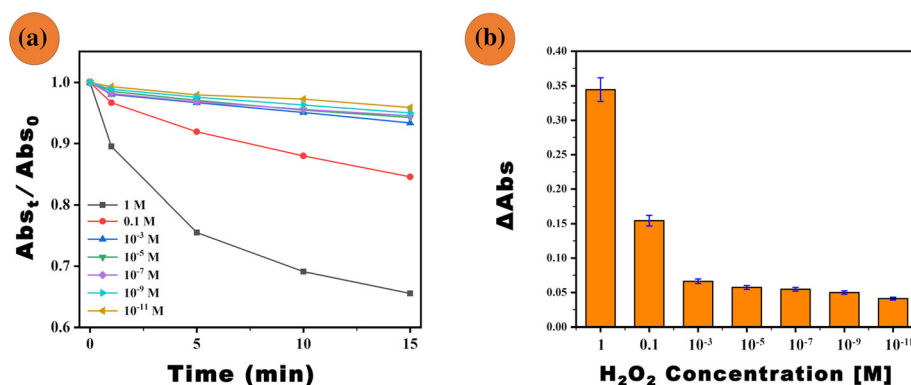
hand, when using lower concentrations of H_2O_2, the solution does not become completely discoloured.

To highlight the response of the CuNPs solution 15 min after addition of H_2O_2, the absorbance variation ($\Delta Abs = Abs_0 - Abs_t$) as a function of analyte concentration is shown in Fig. 7b.

The CuNPs solution proved capable of detecting H_2O_2 in the concentration ranging from 1 to 10^{-11} M, with a relative standard deviation of approximately 5%. The lowest concentration of the detected H_2O_2 was 10^{-11} M. This result is appreciable as can be seen from the comparison with other works in the literature (Table 1).

The ability of the solution to interact with hydrogen peroxide was assumed to be attributable to the catalytic properties of the copper nanoparticles. When these particles interact with H_2O_2, they decomposed and oxidised to copper ions, producing a visible decolourisation of the solution.

To test this hypothesis, three samples of the CuNPs solution were observed at TEM, labelled S-1, S-2 and S-3, respectively. S-1, used as a reference, contained only the CuNPs solution (Fig. 8a). In contrast, S-2 (Fig. 8a') was observed after the addition of 100 μL of

a 10^{-3} M solution of H_2O_2, while S-3 (Fig. 8a'') was observed after the addition of 100 μL of a 1 M solution of H_2O_2.

These H_2O_2 concentrations were chosen to highlight the effect of its interaction with the copper nanoparticles.

Comparing the three TEM images, it is evident that as the H_2O_2 concentration increases, the metallic copper nanoparticles gradually disappear.

The disgregating process of CuNPs due to the interaction with H_2O_2 was also confirmed by the analysis of the SAED patterns acquired from each sample. While the SAED pattern of S-1 reveals a high degree of crystallinity of the CuNPs shown in Fig. 8b, the SAED patterns of S-2 and S-3 (Fig. 8b', b'', respectively) demonstrate a crystallinity loss of the particles following the progressive interaction with the oxidising analyte. This crystallinity loss can also be seen in the electron diffraction profiles obtained from the SAED patterns using the PASAD plug-in of the Gatan Microscopy Suite® software. From the comparison of the electron diffraction profiles shown in Fig. 8c, c', c'', it is evident that as the concentration of hydrogen peroxide increases, the contribution of the crystalline phase considerably decreases until it is no longer present in S-3.

Conclusion

The colloidal CuNPs solution produced in this work was synthesised using a wet synthesis protocol. Morphological and structural analyses by TEM enabled the size distribution of CuNPs to be determined and SAED analyses showed the absence of copper oxide nanoparticle traces. Considering the tendency of copper to oxidise, this result is

Table 1 Comparison of the analytical performance of our CuNPs solution with some sensors reported in the literature based on CuNPs for the detection of H_2O_2

References	L.O.D [M]	Analytical method
[39]	$4.4 \cdot 10^{-5}$	Optical
[40]	$5.5 \cdot 10^{-7}$	Optical
[41]	$1.4 \cdot 10^{-6}$	Amperometric
[42]	$3.4 \cdot 10^{-6}$	Amperometric
[43]	$6.0 \cdot 10^{-7}$	Electrochemical
This work	10^{-11}	Optical
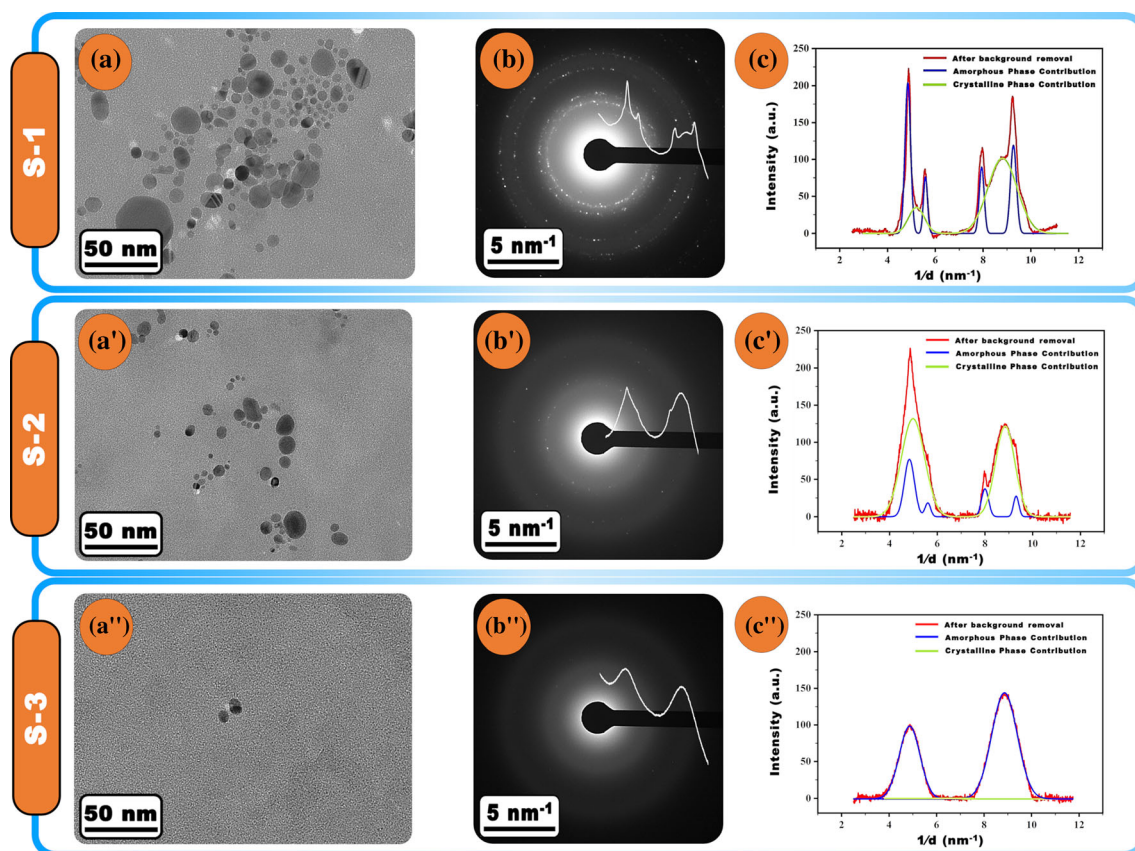
Figure 8 TEM images (**a**, **a′** and **a″**), SAED patterns (**b**, **b′** and **b″**) with PASAD profiles superimposed in white and electron diffraction profiles (**c**, **c′** and **c″**) of S-1, S-2 and S-3.

significant. In addition, the solution proved to be stable over time thanks to the stabilizing action of Tween® 60 and the antioxidant action of ascorbic acid.

Tests on the CuNPs solution ability to detect H_2O_2 revealed a high sensitivity with a detection limit of 10^{-11} M. This is certainly a great advantage in terms of performance of a potential sensor for H_2O_2. However, selectivity needs to be demonstrated by further tests in the future.

Author contributions

AS and DM designed the research, performed the calculations and the morphological characterization, GGC and AB performing the experimental synthesis and optical characterization, analysed the results and wrote the manuscript. All authors contributed the discussions.

Declarations

Conflict of interest The authors declare that they have no known competing financial interests or personal relationships that could have appeared to influence the work reported in this paper.

References

[1] Apel K, Hirt H (2004) Reactive oxygen species: metabolism, oxidative stress, and signal transduction. Annu Rev Plant Biol 55:373–399. https://doi.org/10.1146/annurev.arplant.55.031903.141701

[2] Ray PD, Huang BW, Tsuji Y (2012) Reactive oxygen species (ROS) homeostasis and redox regulation in cellular signaling. Cell Signal 24:981–990

[3] Silva RAB, Montes RHO, Richter EM, Munoz RAA (2012) Rapid and selective determination of hydrogen peroxide residues in milk by batch injection analysis with amperometric detection. Food Chem 133:200–204. https://doi.org/10.1016/j.foodchem.2012.01.003

[4] Gimeno P, Bousquet C, Lassu N et al (2015) High-performance liquid chromatography method for the determination of hydrogen peroxide present or released in teeth bleaching kits and hair cosmetic products. J Pharm Biomed Anal 107:386–393. https://doi.org/10.1016/j.jpba.2015.01.018

[5] Matos RC, Pedrotti JJ, Angnes L (2001) Flow-injection system with enzyme reactor for differential amperometric determination of hydrogen peroxide in rainwater. Anal Chim Acta 441:73–79. https://doi.org/10.1016/S0003-2670(01)01094-7

[6] Sies H, Berndt C, Jones DP (2017) Oxidative stress. Annu Rev Biochem 86:715–748. https://doi.org/10.1146/annurev-biochem-061516-045037

[7] Liu X, Feng H, Zhang J et al (2012) Hydrogen peroxide detection at a horseradish peroxidase biosensor with a Au nanoparticle-dotted titanate nanotube|hydrophobic ionic liquid scaffold. Biosens Bioelectron 32:188–194. https://doi.org/10.1016/j.bios.2011.12.002

[8] Razola SS, Ruiz BL, Diez NM et al (2002) Hydrogen peroxide sensitive amperometric biosensor based on horseradish peroxidase entrapped in a polypyrrole electrode. Biosens Bioelectron 17:921–928. https://doi.org/10.1016/S0956-5663(02)00083-0

[9] Lei CX, Hu SQ, Shen GL, Yu RQ (2003) Immobilization of horseradish peroxidase to a nano-Au monolayer modified chitosan-entrapped carbon paste electrode for the detection of hydrogen peroxide. Talanta 59:981–988. https://doi.org/10.1016/S0039-9140(02)00641-0

[10] Wen F, Dong Y, Feng L et al (2011) Horseradish peroxidase functionalized fluorescent gold nanoclusters for hydrogen peroxide sensing. Anal Chem 83:1193–1196. https://doi.org/10.1021/ac1031447

[11] Navas Díaz A, Ramos Peinado MC, Torijas Minguez MC (1998) Sol-gel horseradish peroxidase biosensor for hydrogen peroxide detection by chemiluminescence. Anal Chim Acta 363:221–227. https://doi.org/10.1016/S0003-2670(98)00080-4

[12] Hermanson GT (2013) Bioconjugate Techniques, 3rd edn. Elsevier, Amsterdam

[13] Carbone GG, Serra A, Buccolieri A, Manno D (2019) A silver nanoparticle-poly(methyl methacrylate) based colorimetric sensor for the detection of hydrogen peroxide. Heliyon 5:e02887. https://doi.org/10.1016/j.heliyon.2019.e02887

[14] Sepúlveda B, Angelomé PC, Lechuga LM, Liz-Marzán LM (2009) LSPR-based nanobiosensors. Nano Today 4:244–251

[15] Petryayeva E, Krull UJ (2011) Localized surface plasmon resonance: nanostructures, bioassays and biosensing—a review. Anal Chim Acta 706:8–24

[16] Hu M, Chen J, Li ZY et al (2006) Gold nanostructures: engineering their plasmonic properties for biomedical applications. Chem Soc Rev 35:1084–1094. https://doi.org/10.1039/b517615h

[17] Rycenga M, Cobley CM, Zeng J et al (2011) Controlling the synthesis and assembly of silver nanostructures for plasmonic applications. Chem Rev 111:3669–3712

[18] Hossein Habibi M, Kamrani R, Mokhtari R (2010) Fabrication and characterization of copper nanoparticles using thermal reduction: the effect of nonionic surfactants on size and yield of nanoparticles. Microchim Acta 171:91–95. https://doi.org/10.1007/s00604-010-0413-2

[19] Lassègue P, Noé L, Monthioux M, Caussat B (2017) Fluidized bed chemical vapor deposition of copper nanoparticles on multi-walled carbon nanotubes. Surf Coat Technol 331:129–136. https://doi.org/10.1016/j.surfcoat.2017.10.046

[20] Joshi SS, Patil SF, Iyer V, Mahumuni S (1998) Radiation induced synthesis and characterization of copper nanoparticles. Nanostruct Mater 10:1135–1144. https://doi.org/10.1016/S0965-9773(98)00153-6

[21] Qi L, Ma J, Shen J (1997) Synthesis of copper nanoparticles in nonionic water-in-oil microemulsions. J Colloid Interface Sci 186:498–500. https://doi.org/10.1006/jcis.1996.4647

[22] Tilaki RM, Zad AI, Mahdavi SM (2007) Size, composition and optical properties of copper nanoparticles prepared by laser ablation in liquids. Appl Phys A Mater Sci Process 88:415–419. https://doi.org/10.1007/s00339-007-4000-2

[23] Khanna PK, Gaikwad S, Adhyapak PV et al (2007) Synthesis and characterization of copper nanoparticles. Mater Lett 61:4711–4714. https://doi.org/10.1016/j.matlet.2007.03.014

[24] Guerrini L, Alvarez-Puebla R, Pazos-Perez N (2018) Surface modifications of nanoparticles for stability in biological fluids. Materials 11:1154. https://doi.org/10.3390/ma11071154

[25] Tamayo L, Palza H, Bejarano J, Zapata PA (2019) 8 - Polymer composites with metal nanoparticles: synthesis, properties, and applications. In: Pielichowski K, Majka TM (eds) Polymer composites with functionalized nanoparticles. Elsevier, pp 249–286

[26] Kaur G, Mehta SK (2017) Developments of Polysorbate (Tween) based microemulsions: preclinical drug delivery, toxicity and antimicrobial applications. Int J Pharm 529:134–160

[27] Aslan K, Pérez-Luna VH (2002) Surface modification of colloidal gold by chemisorption of alkanethiols in the presence of a nonionic surfactant. Langmuir 18:6059–6065. https://doi.org/10.1021/la025795x

[28] Yabuki A, Tanaka S (2011) Oxidation behavior of copper nanoparticles at low temperature. Mater Res Bull

Springer

46:2323–2327. https://doi.org/10.1016/j.materresbull.2011.08.043

[29] Dang TMD, Le TTT, Fribourg-Blanc E, Dang MC (2011) Synthesis and optical properties of copper nanoparticles prepared by a chemical reduction method. Adv Nat Sci Nanosci Nanotechnol 2:015009. https://doi.org/10.1088/2043-6262/2/1/015009

[30] Njus D, Kelley PM, Tu Y-J, Schlegel HB (2020) Ascorbic acid: the chemistry underlying its antioxidant properties. Free Radical Biol Med 159:37–43. https://doi.org/10.1016/j.freeradbiomed.2020.07.013

[31] Liu QM, Yasunami T, Kuruda K, Okido M (2012) Preparation of Cu nanoparticles with ascorbic acid by aqueous solution reduction method. Trans Nonferr Met Soc China (English Edition) 22:2198–2203. https://doi.org/10.1016/S1003-6326(11)61449-0

[32] Szymczyk K, Szaniawska M, Taraba A (2018) Micellar parameters of aqueous solutions of Tween 20 and 60 at different temperatures: volumetric and viscometric study. Colloids Interfaces 2:34. https://doi.org/10.3390/colloids2030034

[33] Hergert W, Wriedt T (2012) The Mie theory. Springer, Berlin Heidelberg

[34] Yang JS, Lee SG, Park S-G et al (2009) Drude model for the optical properties of a nano-scale thin metal film revisted. J Korean Phy Soc 55:2552–2555. https://doi.org/10.3938/jkps.55.2552

[35] Johnson PB, Christy RW (1972) Optical constants of the noble metals. Phys Rev B 6:4370–4379. https://doi.org/10.1103/PhysRevB.6.4370

[36] Zhao Y, Wang Z, Zhang W, Jiang X (2010) Adsorbed Tween 80 is unique in its ability to improve the stability of gold nanoparticles in solutions of biomolecules. Nanoscale 2:2114-2119. https://doi.org/10.1039/c0nr00309c

[37] Mahapatra O, Bhagat M, Gopalakrishnan C, Arunachalam KD (2008) Ultrafine dispersed CuO nanoparticles and their antibacterial activity. J Exp Nanosci 3:185–193. https://doi.org/10.1080/17458080802395460

[38] Chand Mali S, Raj S, Trivedi R (2019) Biosynthesis of copper oxide nanoparticles using Enicostemma axillare (Lam.) leaf extract. Biochem Biophys Rep 20:100699. https://doi.org/10.1016/j.bbrep.2019.100699

[39] Zarif F, Khurshid S, Muhammad N et al (2020) Colorimetric sensing of hydrogen peroxide using ionic-liquid-sensitized zero-valent copper nanoparticle (nZVCu). ChemistrySelect 5:6066–6074. https://doi.org/10.1002/slct.202001470

[40] Mao Z, Qing Z, Qing T et al (2015) Poly(thymine)-templated copper nanoparticles as a fluorescent indicator for hydrogen peroxide and oxidase-based biosensing. Anal Chem 87:7454–7460. https://doi.org/10.1021/acs.analchem.5b01700

[41] Liu Y, Han Y, Chen R et al (2016) In situ immobilization of copper nanoparticles on polydopamine coated graphene oxide for H_2O_2 determination. PLoS ONE 11:e0157926. https://doi.org/10.1371/journal.pone.0157926

[42] Sophia J, Muralidharan G (2015) Amperometric sensing of hydrogen peroxide using glassy carbon electrode modified with copper nanoparticles. Mater Res Bull 70:315–320. https://doi.org/10.1016/j.materresbull.2015.04.058

[43] Moozarm Nia P, Woi PM, Alias Y (2017) Facile one-step electrochemical deposition of copper nanoparticles and reduced graphene oxide as nonenzymatic hydrogen peroxide sensor. Appl Surf Sci 413:56–65. https://doi.org/10.1016/j.apsusc.2017.04.043